

Published in final edited form as:

*Acc Chem Res.* 2007 July ; 40(7): 581–591. doi:10.1021/ar600060t.

## O<sub>2</sub> and N<sub>2</sub>O Activation by Binuclear, Trinuclear, and Tetranuclear Cu Clusters in Biology

Edward I. Solomon, Ritimukta Sarangi, Julia S. Woertink, Anthony J. Augustine, Jungjoo Yoon, and Somdatta Ghosh

*Department of Chemistry, Stanford University, Stanford, California 94305*

### Abstract

Copper cluster sites in biology exhibit unique spectroscopic features reflecting exchange coupling between oxidized Cu's and e<sup>-</sup> delocalization in mixed valent sites. These novel electronic structures play critical roles in O<sub>2</sub> binding and activation for electrophilic aromatic attack and H atom abstraction, the 4e<sup>-</sup>/4H<sup>+</sup> reduction of O<sub>2</sub> to H<sub>2</sub>O, and in the 2e<sup>-</sup>/2H<sup>+</sup> reduction of N<sub>2</sub>O. These electronic structure/reactivity correlations are summarized below.

Cu proteins play central roles in Fe, Cu, and O<sub>2</sub> metabolism, are related to a range of genetic diseases and are important in biotechnology, detoxification, and the elimination of greenhouse gases. Understanding Cu biochemistry on a molecular level provides mechanisms to improve or inhibit these processes and enhance drug design. The Cu proteins involved in O<sub>2</sub> binding, activation, reduction to H<sub>2</sub>O and the reduction of N<sub>2</sub>O to water and dinitrogen are summarized in Figure 1. The term “coupled” is used here to refer to the antiferromagnetic (AF) “coupling” between paramagnetic metal centers that can lead to a diamagnetic S<sub>tot</sub>=0 ground state. If two Cu(II)'s, S=1/2, directly overlap they will spin pair. If, however, they are far enough apart so that their d orbitals do not directly overlap but have a bridging ligand this can provide a superexchange pathway (i.e. a delocalized molecular orbital) between the two paramagnetic Cu(II)'s that results in their spin pairing, indirectly through overlap with the bridge. This is described by the exchange Hamiltonian  $H = -2JS_A \cdot S_B$  which spin couples the two S=1/2's on Cu<sub>A</sub> and Cu<sub>B</sub> to form total spins S<sub>tot</sub>=1 and 0 where for AF coupling the S<sub>tot</sub>=0 is lower in energy by 2J (J<0).

In this paper we will: 1) consider the unique spectral features of the coupled binuclear Cu proteins, hemocyanin (Hc), catechol oxidase, and tyrosinase (Ty), that reflect a novel electronic structure that allows their reversible binding of O<sub>2</sub> (a spin forbidden process) and its activation for electrophilic attack on an aromatic substrate by Ty; 2) contrast this electronic structure to that of the non-coupled binuclear Cu enzymes (i.e. no magnetic interaction between the two Cu(II)'s S=1/2) to evaluate the contribution of these differences in AF exchange coupling to the reaction mechanisms, where the non-coupled binuclear Cu sites in dopamine α-monooxygenase (DβM) and peptidylglycine α-hydroxylating monooxygenase (PHM) activate O<sub>2</sub> for H-atom abstraction; 3) Extend these studies to the trinuclear Cu cluster site in the multicopper oxidases, where the exchange coupling among the three coppers plays a central role in the 4e<sup>-</sup>/4H<sup>+</sup> reduction of O<sub>2</sub> to H<sub>2</sub>O; and 4) Consider how the interactions among the coppers in the μ<sub>4</sub> sulfide bridged tetranuclear Cu<sub>4</sub> cluster promote the 2e<sup>-</sup>/2H<sup>+</sup> cleavage of the N-O bond by N<sub>2</sub>O reductase.

Correspondence to: Edward I. Solomon.

Ritimukta Sarangi, Julia Woertink, Anthony Augustine, Jungjoo Yoon, and Somdatta Ghosh are all graduate students in the lab of Edward I. Solomon, who is the Monroe E. Spaght Professor of Chemistry at Stanford University

## 1. Coupled Binuclear Copper Proteins

From spectroscopy and crystallography, Hc (reversible O<sub>2</sub> binding), catechol oxidase (O<sub>2</sub> binding and catechol oxidation to quinone) and Ty (O<sub>2</sub> binding, oxidation and monooxygenation of phenol to catechol) all have equivalent geometries ( $\mu\text{-}\eta^2\text{:}\eta^2$  Cu(II)<sub>2</sub>O<sub>2</sub>, side-on peroxide bridged binuclear Cu(II) sites coordinated to the protein by 3 His ligands on each Cu) and electronic structures (*vide infra*).<sup>1</sup> Their range of functions increases from Hc to Ty, which has been attributed to differences in substrate accessibility to their coupled binuclear Cu sites.

### 1.1 Unique Spectroscopic Features → Novel Electronic Structure

To understand the unique spectral features of the oxygenated sites of these proteins we first consider what is normal for a Cu(II)-peroxide bond. Cu(II) is d<sup>9</sup> and thus has one half occupied valence d-orbital, either  $d_{x^2-y^2}$  for tetragonal or  $d_z^2$  for trigonal bipyramidal geometries. Peroxide has a doubly degenerate highest occupied molecular orbital (HOMO) set which will split in energy upon binding to Cu(II), the  $\pi^*_\sigma$  being stabilized to deeper binding energy due to  $\sigma$  bonding to the half occupied d orbital and the  $\pi^*_\nu$  (vertical) not being very affected by bonding as it is perpendicular to the Cu(II)-(O<sub>2</sub><sup>2-</sup>)plane (Figure 2A).<sup>2</sup>

In a peroxide bridged binuclear Cu(II) complex as in the [(TPMA)Cu]<sub>2</sub>O<sub>2</sub> dimer (trigonal bipyramidal at each Cu(II)), one further has to take symmetric and antisymmetric combinations of the half occupied  $d_z^2$  orbitals on the Cu's and then allow for bonding with the occupied peroxide  $\pi^*_\sigma$  valence orbitals.<sup>3</sup> As shown in Figure 2B only one contribution of  $d_z^2$  orbitals has net  $\sigma$  overlap with the peroxide  $\pi^*_\sigma$  orbital causing stabilization of the  $\pi^*_\sigma$  orbital and a destabilization of the  $d_z^2_A + d_z^2_B$  molecular orbital. This leads to spin pairing of the two electrons in the  $d_z^2$  orbitals of the two coppers and the antiferromagnetically coupled S=0, singlet ground state. This also produces a peroxide  $\pi^*_\sigma \rightarrow \text{Cu}(d_z^2_A + d_z^2_B)$  charge transfer (CT) transition as shown in Figure 3A. Resonance Raman (rR) excitation into this CT transition produces an O-O stretching vibration at ~830 cm<sup>-1</sup> (Figure 3B) which is characteristic of peroxide bridging in a "normal" binuclear Cu(II) complex.<sup>3</sup>

We now consider the unique geometric and electronic structure of oxy-Hc/Oxy-Ty. Again, we take the symmetric and antisymmetric combination of the  $d_{x^2-y^2}$  half occupied valence orbitals of the two coppers (here the ligand field of each Cu is square pyramidal) and allow for their bonding interactions with the peroxide  $\pi^*$  valence orbitals, but in the side-on peroxide bridged structure of the oxy-Hc site (Figure 2C). Again the  $\pi^*_\sigma$  orbital is stabilized and the Cu  $d_{x^2-y^2_A} + d_{x^2-y^2_B}$  is destabilized due to  $\sigma$  bonding. However, in the side-on bridged structure there are two  $\sigma$ -bonding interactions of the peroxide with each copper and this leads to a very large bonding-antibonding interaction.<sup>4</sup> Thus, a strongly AF stabilized singlet ground state and an intense O<sub>2</sub><sup>2-</sup>  $\pi^*_\sigma \rightarrow \text{Cu}(d_{x^2-y^2_A} + d_{x^2-y^2_B})$  CT transition, which is shifted to higher energy, are observed (Figure 3A, green vs. black). Importantly, rR excitation into this CT transition shows a very low O-O stretching frequency ( $\nu_{\text{O-O}}$ ) at ~750 cm<sup>-1</sup> (Figure 3B). The large peroxide  $\sigma$  donation of electron density from the  $\pi^*_\sigma$  orbital (which is antibonding with respect to the O-O bond) to the Cu(II)'s should increase not decrease the strength of the O-O bond. However, there is an additional bonding interaction that occurs in the side-on peroxide bridged structure. The LUMO on the peroxide is the  $\sigma^*$  (Figure 2C) which bonds with the occupied  $d_{x^2-y^2_A} + d_{x^2-y^2_B}$  combination of d-orbitals on the Cu's which is the HOMO. This back-bonding shifts some of the electron density into the O<sub>2</sub><sup>2-</sup>  $\sigma^*$  orbital which is strongly antibonding with respect to the O-O bond and leads to the very low  $\nu_{\text{O-O}}$ .<sup>4</sup>

In summary, the extremely covalent  $\sigma$  bonding between the two Cu(II)'s through the  $\mu\text{-}\eta^2\text{:}\eta^2$  peroxide  $\pi^*_\sigma$  orbital leads to the AF coupled singlet ground state and the backbonding of

electron density from the Cu ( $d_x^2-y^2_A + d_x^2-y^2_B$ ) HOMO into the peroxide  $\sigma^*$  LUMO leads to an extremely weak O-O bond activated for cleavage.

## 1.2 Reaction Coordinate for O<sub>2</sub> Binding

DeoxyHc/Ty with two  $d^{10}$  Cu(I) centers binds triplet O<sub>2</sub> reversibly to form oxyHc/oxyTy which has the AF coupled singlet ground state. Thus, this reaction is spin forbidden. To obtain a reaction coordinate for reversible O<sub>2</sub> binding, we started with the  $\mu\text{-}\eta^2\text{:}\eta^2$  structure, moved the peroxide out of the molecular plane, and geometry optimized the rest of the structure.<sup>5</sup> The structure first butterflies, then goes to a  $\mu\text{-}\eta^1\text{:}\eta^2$  asymmetric structure, and then to an end-on bridged structure in the reversible loss of O<sub>2</sub> (Figure 4A). These structures maximize the metal-ligand overlaps along this reaction coordinate. As the peroxide moves away from the coppers, its negative charge decreases as does the positive charge on the coppers. Thus, electron density is being transferred from the peroxide to the Cu(II)'s. Importantly, both coppers are reduced at the same rate even in the asymmetric  $\mu\text{-}\eta^1\text{:}\eta^2$  structure. Thus, the reversible loss of peroxide as O<sub>2</sub> involves simultaneous two electron transfer.

In Figure 4B we consider how the spin changes along this reaction coordinate. On the far left is the AF stabilization of the singlet ground state of the side-on peroxide bridged structure through its  $\pi^*_\sigma$  orbital. However, as the peroxide moves out of the molecular plane to the butterflyed structure, the singlet/triplet splitting collapses and the triplet is in fact slightly lower in energy. This is because the spin on each Cu covalently delocalizes into a different peroxide  $\sigma^*$  orbital. These are close to orthogonal in the butterflyed structure which favors the triplet ground state. From here, one electron of the same spin can be transferred from each  $\sigma^*$  orbital to each Cu leading to loss of O<sub>2</sub> in its triplet  $^3\Sigma_g^-$  ground state.<sup>5</sup>

Thus, the stabilization of the triplet ground state of O<sub>2</sub> is lost by charge transfer from the remote Cu's and the singlet structure is then stabilized by the formation of an efficient superexchange pathway (the  $\pi^*_\sigma$  orbital overlap) along the reaction coordinate.

## 1.3 Reaction Coordinate of Monooxygenation

In early literature we found that oxyTy had the same geometric and electronic structure as oxyHc but that it differed for Hc in having substrate access and coordination directly to the copper in a trigonal bipyramidal distorted structure. This led to the generally accepted monooxygenation mechanism for oxyTy shown in Figure 5.<sup>1,6,7</sup> Phenolate substrate binds directly to the side-on peroxy bridged oxyTy site (oxy-T). The trigonal pyramidal distortion leads to electrophilic attack and hydroxylation at the ortho-position to produce a bound catecholate (met-D). Two electron oxidation leads to the corresponding quinone product and a reduced (deoxy) site capable of O<sub>2</sub> binding for further turnover. The interesting issue now is whether the side-on oxyTy structure directly reacts with the aromatic ring or whether phenolate coordination leads to a bis- $\mu$  oxo structure (*vide infra*) and this does the electrophilic attack on the ring.

The latter possibility was raised by the results of Tolman *et al.* who showed that the side-on peroxy bridged structure could convert to the bis- $\mu$  oxo structure with certain chelating ligands (Figure 6A).<sup>8</sup> Cu K pre-edge X-ray absorption data showed that conversion of the side-on to the bis- $\mu$  oxo isomer leads to an increase in energy of the Cu 1s $\rightarrow$ 3d transition by 1.9 eV indicating that the Cu(II) is oxidized to Cu(III) in the bis- $\mu$  oxo structure.<sup>9</sup> The orbital correlation diagram for this interconversion is given in Figure 6B. Starting from the side-on bridged structure on the left, the O-O bond elongates from 1.4 Å to 2.3 Å in the bis- $\mu$  oxo structure (the Cu-O distance goes from 1.92 to 1.81 Å). The O<sub>2</sub><sup>2-</sup>  $\sigma^*$  orbital thus drops in energy to below the HOMO on the coppers resulting in oxidation to two Cu(III)'s and reduction of the peroxide to the bridged oxide level.<sup>10</sup> This produces a low energy intense  $\mu\text{-O}^{2-} \rightarrow \text{Cu}$

( $d_x^2-y^2_A - d_x^2-y^2_B$ ) LUMO CT transition (Figure 3A, blue), and rR excitation into this transition now shows an intense vibrational peak at  $600\text{ cm}^{-1}$  corresponding to the  $\text{Cu}_2(\text{O})_2$  symmetric stretch (Figure 3B). Thus, we now have two LUMO's that are frontier molecular orbitals (FMO) capable of electrophilic attack on the occupied  $\pi$  orbitals of the aromatic ring (Figure 6C). In the side-on bridged structure, there is a Cu LUMO with significant peroxide  $\pi^*_\sigma$  character due to the strong donor interaction of the peroxide with the Cu. In the bis- $\mu$  oxo structure, the Cu based LUMO now has significant  $\sigma^*$  character due to the strong oxide  $\sigma$  donor interaction.

From model studies, both the  $\pi^*$  LUMO of the side-on peroxide and the  $\sigma^*$  LUMO of the bis- $\mu$  oxo structures are capable of electrophilic reactions with aromatic substrates. From Figure 7A, in the Karlin bidentate chelate ligand system<sup>11</sup>, an  $\text{O}_2$  intermediate is trapped at low temperature with an electron withdrawing nitro substituent on the bridging ring. From rR data (Figure 7B), this species shows a  $\sim 750\text{ cm}^{-1}$  vibration characteristic of the side-on peroxo bridged species with no indication of a  $600\text{ cm}^{-1}$  feature characteristic of the bis- $\mu$  oxo species (upper limit of  $< 0.1\%$ ).<sup>12</sup> As shown in Figures 7B and 7C, the  $\sim 750\text{ cm}^{-1}$  feature decreases as the  $1320\text{ cm}^{-1}$  feature, characteristic of the C-O stretch of the hydroxylated phenolate product, increases.

From Figure 8, the Stack diamine ligated complex binds  $\text{O}_2$  as the side-on peroxo bridged species.<sup>13</sup> Addition of exogenous phenolate leads to the loss of the  $\sim 750\text{ cm}^{-1}$   $\nu_{\text{O-O}}$  vibration and appearance of the  $600\text{ cm}^{-1}$  feature characteristic of the bis- $\mu$  oxo species. Thus, coordination of the phenolate to the Cu likely through a trigonal bipyramidal rearrangement into the equatorial plane, converts the side-on peroxide to the bis- $\mu$  oxo species. This goes on to hydroxylate the phenolate to a mixture of catechol and quinone products. Thus, both the side-on peroxo (through a  $\pi^*$  electrophilic mechanism) and the bis- $\mu$  oxo (through a  $\sigma^*$  electrophilic mechanism) binuclear Cu sites can hydroxylate aromatic substrates.

## 2. Non-coupled Binuclear Cu Enzymes

PHM and D $\beta$ M, involved in peptidic hormone production and the control of neurotransmitters, both catalyze substrate C-H bond hydroxylation by H-atom abstraction.<sup>14</sup> The active sites in these enzymes are non-coupled in that they have two Cu(II)'s which each show spectroscopic features indicative of an isolated Cu(II)  $S=1/2$  center. This is consistent with the crystallography on PHM which shows that the two Cu(II)'s are  $11\text{ \AA}$  apart with no bridging ligation (only  $\text{H}_2\text{O}$ s in the interdomain cavity between the Cu's).<sup>15</sup> Reasonable descriptions of the geometric and electronic structure of each Cu(II) center have been obtained through a combination of crystallography, EXAFS, MCD spectroscopy and DFT calculations.<sup>16,17</sup> As shown in Figure 9  $\text{Cu}_M$  is the catalytic center which has an axial Met, two equatorial His and two equatorial  $\text{H}_2\text{O}/\text{OH}^-$  sites for  $\text{O}_2$  reactivity.  $\text{Cu}_H$  has 3 His and a water ligand in a  $D_{2d}$  distorted tetragonal geometry and supplies the extra  $e^-$  required for catalysis to  $\text{Cu}_M$  over a distance of  $11\text{ \AA}$ . There has been much discussion as to how this ET might take place.<sup>18</sup>

Thus the reaction of the non-coupled binuclear Cu enzymes requires  $\text{O}_2$  activation by a single Cu center, which until recently was thought to involve a  $\text{Cu}_M(\text{II})\text{-OOH}$  species.<sup>14</sup> However from spectroscopic and electronic structure studies on a Cu(II)-hydroperoxide model complex, this species is not activated for H-atom abstraction.<sup>19</sup> From Figure 10A the FMO only has 2% character on the distal oxygen for electrophilic attack and from rR studies on the model the  $\nu_{\text{O-O}}$  is  $843\text{ cm}^{-1}$  reflecting a strong O-O bond not activated for cleavage. This led us to studies of the alternative possibility of a  $1e^-$  reduction of  $\text{O}_2$  to generate a bound superoxo- $\text{Cu}_M(\text{II})$  intermediate. From the rR data in Figure 10B the  $\nu_{\text{O-O}}$  of an  $\eta^2\text{O}_2\text{Cu}$  model complex is  $1043\text{ cm}^{-1}$  which is characteristic of a Cu(II)- $\text{O}_2^-$  species; from its FMO which has  $>60\%$  O character this species is strongly activated for electrophilic attack on H-C bonds.<sup>20</sup>

These predictions from model studies were strongly supported by electronic structure calculations of this reaction coordinate.<sup>21</sup> H atom abstraction by the  $2e^-$  reduced  $Cu_M(II)$ -hydroperoxo species (Figure 11 blue) is endergonic and in particular has an activation barrier of 37 kcal/mol. Alternatively H atom abstraction by the  $1e^-$  reduced Cu-superoxo species (Figure 11 red) is thermoneutral and has an activation barrier of only 14 kcal/mol, which is consistent with the FMO predictions. This would generate a  $Cu_M(II)$ -OOH and substrate radical species, which would readily react via direct OH transfer from the hydroperoxide to generate the hydroxylated product and a  $Cu_M(II)$ -O $^-$  (i.e. cupric-oxy) species. This high energy species would drive a proton coupled ET from  $Cu_H$  to complete the reaction cycle.

A comparison of the reaction coordinates for the coupled binuclear Cu enzymes (Figure 5) and non-coupled binuclear Cu enzymes (Figure 11) shows an extremely important role of the differences in the AF exchange coupling ( $J$ ) in the reaction mechanism. Rapid ET requires a large electronic coupling between the donor and acceptor ( $H_{DA}$ ) which in turn is related to  $J\alpha$  ( $H_{DA}$ )<sup>2,21</sup>. Thus large AF coupling leads to rapid ET. This is the case for the coupled binuclear Cu enzymes where the large value of  $J$  between the Cu's via the bridging ligand leads to the  $2e^-$  reduction of  $O_2$  to form a  $Cu_2O_2$  species capable of electrophilic aromatic attack. Alternatively in these non-coupled binuclear Cu enzymes  $J$  is very small as  $Cu_M$  and  $Cu_H$  are separated by an 11 Å solvent-filled cleft. The reduction appears to proceed at one Cu via a  $1e^-$  reduced  $Cu_M(II)$ - $O_2^-$  species which is capable of H atom abstraction. Such a  $Cu_MO_2$  species has been observed in the crystal structure of PHM<sup>22</sup> and defined by  $rR$  in a model complex.<sup>23</sup> At a later stage of the reaction a high energy species is produced (the  $Cu_M(II)$ -oxy) which provides the large driving force required for ET from  $Cu_H$  with its low  $J$  (therefore  $H_{DA}$ ) with  $Cu_M$ .

### 3. Trinuclear Cu Cluster in the Multicopper Oxidases (MCOs)

The MCOs couple four  $1e^-$  oxidations of substrates to the  $4e^-/4H^+$  reduction of  $O_2$  to  $H_2O$ .<sup>1</sup> These can be divided into two classes: one as represented by laccase uses organic substrates which weakly to strongly interact with the protein near the type 1 (T1) Cu (vide infra) and the second represented by Fet3p has specific metal ion substrate binding sites near the T1 which tune the metal ion potential and provide ET pathways to the T1.<sup>24</sup> The minimum structure of a MCO active site is shown in Figure 12A.

The T1 is a blue copper center capable of rapid ET through a Cys-His pathway over 13 Å to the trinuclear Cu cluster (TNC) where  $O_2$  is reduced to  $H_2O$ . The TNC is comprised of a type 3 (T3) copper pair, where each Cu has three His ligands and the pair is strongly antiferromagnetically coupled (i.e. with a singlet ground state) through an  $OH^-$  bridge, and a type 2 (T2) center within 3.5 Å of the T3 Cu's having two His and a  $OH^-$  ligand external to the cluster.<sup>25</sup> The T2 Cu is not bridged to the T3 Cu's and shows a normal Cu(II)  $S=1/2$  EPR signal.

The electronic structure of the resting trinuclear Cu(II) cluster is given in Figure 12B. This shows that all three Cu's have open coordination positions oriented inside the cluster. The coordination unsaturation of this highly positively charged cluster results from charged carboxylate residues within 8 Å of the cluster which destabilize  $H_2O/OH^-/O_2^-$  binding in the center of the cluster and thus tune its redox properties for  $O_2$  reduction.<sup>26</sup>

$O_2$  intermediates were trapped to define the mechanism of  $O_2$  reduction to  $H_2O$  by the MCOs. Initially, we studied a T1 depleted (T1D) derivative in laccase where the T1 Cu was replaced by a redox inactive  $Hg^{2+}$ .<sup>27</sup> Reduction of the TNC and reaction with  $O_2$  led to the first intermediate. From a combination of isotope ratio mass spectrometry, CD, and LT MCD (which only probes paramagnetic centers), we determined that this was a peroxy intermediate with

two coppers oxidized and AF coupled and one copper reduced.<sup>27</sup> The AF coupling required bridging ligation and this was observed in EXAFS data on peroxy T1D, which showed two Cu's tightly bridged at 3.4 Å. Since one Cu was reduced in this intermediate, we could not directly study its interaction with the peroxide. So we prepared the peroxide adduct (PA) of the oxidized TNC in T1D.<sup>28</sup> PA showed the same FT-EXAFS feature at 3.4 Å indicating a similar peroxide binding mode but now all Cu's are oxidized. On binding peroxide to the oxidized TNC all the ligand field features of the T2 and T3 Cu(II)'s are perturbed, indicating an all bridged structure for the peroxide intermediate. This is consistent with the recent crystal structure of the peroxide adduct of oxidized CotA<sup>29</sup> and the QM/MM energy minimized structure of the peroxide intermediate.<sup>30</sup>

Reaction of the fully reduced native enzyme (i.e. 4Cu(I)) with O<sub>2</sub> generates the native intermediate (NI). As shown in Figure 13A, NI exhibits absorption features at 365 and 318 nm as well as an absorption band at 600 nm associated with an oxidized T1 Cu.<sup>31</sup> Therefore NI is at least one more electron reduced relative to the peroxide intermediate. Associated with this, NI exhibits an unusual EPR signal (Figure 13C) with very unusual g-values below 2.0. It is different from that of an oxidized T2 Cu(II) and broadens when generated with <sup>17</sup>O<sub>2</sub>.<sup>32</sup> Thus, it had been assigned as an OH. bound to a reduced T2 Cu. The most direct spectroscopic probe of reduced Cu is K-edge XAS as Cu(I) exhibits a characteristic feature at 8984 eV not present in Cu(II) complexes. It is also not present in NI.<sup>31</sup> Therefore, NI is a fully oxidized TNC, but with an EPR signal very different from that of the fully oxidized TNC of the resting enzyme (Figure 13C), and dioxygen has been fully reduced to the H<sub>2</sub>O level.

NI also has a characteristic derivative shaped MCD signal associated with the 365/318 nm absorption bands known as a pseudo-A term (Figure 13A).<sup>31</sup> This has proven to be a direct probe of the geometric and electronic structure of NI. The field dependence of the MCD signal at low temperature gave a saturation magnetization curve which fit to the Brillouin function for an S = 1/2 ground state, associated with the unusual g-values. The temperature dependence of the MCD signal at a fixed high magnetic field shows a very interesting behavior in Figure 13B. Normally MCD intensity of a paramagnetic S = 1/2 center decreases as 1/T. However, the MCD intensity in Figure 13B first decreases then increases with increasing temperature indicating Boltzmann population of an excited state at 150 cm<sup>-1</sup> with an MCD signal different from that of the S = 1/2 ground state of NI.

NI has an FT-EXAFS feature indicating a Cu-Cu distance of 3.3 Å, which corresponds to a pair of Cu(II)'s of the trinuclear cluster site having a singlet/triplet splitting of ~520 cm<sup>-1</sup>. Since we are dealing with a trinuclear Cu(II) site, the singlet ground state of the pair couples with the third Cu(II) to give an S<sub>tot</sub> = 1/2 ground state; the S = 1 excited state couples with the S = 1/2 to form S<sub>tot</sub> = 1/2 and 3/2 excited states. With a single bridge, this would produce a T2 EPR signal with g-values above 2.0 and an excited state at 520 cm<sup>-1</sup>. NI has a ground state EPR signal with g-values below 2.0 and an excited state at 150 cm<sup>-1</sup>. Thus we allow for additional AF exchange interactions (i.e. bridging ligands) between additional pairs of Cu(II)'s of the TNC of NI. Allowing for a second bridge splits the excited S<sub>tot</sub> = 3/2 and 1/2 states, but does not bring the S<sub>tot</sub> = 1/2 first excited state below 440 cm<sup>-1</sup> (~1.7J) and does not result in ground state g-values below 2.0. Addition of a third bridge now causes the S = 1/2 excited state to greatly decrease in energy (this is a result of "spin frustration" as all three S = 1/2 cannot be AF coupled in a triangle) and the ground state g-values to decrease below 2.0 (due to antisymmetric exchange in the all bridged trimer).<sup>33</sup> Thus the experimental data on the ground state and excited state of NI require all three Cu(II)'s to be strongly exchange coupled through bridging ligands.

There were two possible structures for NI where all Cu's are oxidized and bridged by the product of full O<sub>2</sub> reduction: a μ<sub>3</sub>-oxo bridged structure, or a tris OH- bridged structure in

which the third  $\text{OH}^-$  would derive from  $\text{H}_2\text{O}$  (Figure 14A top). Model complexes exist with both structures and both exhibit MCD pseudo-A terms (of opposite sign) associated with the hydroxo or oxo to Cu(II) CT transitions of the trinuclear Cu(II) cluster (Figure 14A bottom).<sup>34</sup> The mechanism for pseudo-A terms requires two perpendicular CT transitions being spin-orbit coupled in a third direction at one center. For the tris  $\text{OH}^-$  system, this would involve CT transitions from two  $\text{OH}^-$  ligands to one Cu(II) center which provides the spin-orbit coupling. For the  $\mu_3$ -oxo structure, this involves oxo CT transitions to two Cu(II) centers which are spin-orbit coupled by the oxo bridge. From the temperature dependent MCD spectrum of NI shown in Figure 14B, the CT transitions forming the pseudo-A term involve different Cu centers which is only consistent with a  $\mu_3$ -oxo, all-bridged structure for NI.

The above spectroscopic studies of  $\text{O}_2$  intermediates in the MCO's have led to the molecular mechanism of  $\text{O}_2$  reduction to  $\text{H}_2\text{O}$  in Figure 15. The reduction of  $\text{O}_2$  by the fully reduced MCO involves two  $2e^-$  steps. From our kinetic studies the first is rate determining and the second is fast, therefore it is effectively a  $4e^-$  process.<sup>1</sup> The second step involves the  $2e^-$  reductive cleavage of the O-O bond. It has a large driving force due to the  $2e^-$  reduction potential of peroxide and from mutagenesis studies it is proton assisted with a Glu near the T3 providing the proton for O-O bond cleavage. The NI is a fully oxidized form of the enzyme but is different from the resting form as it has an internal  $\mu_3$ -oxo bridge. These interconvert and the rate of decay of NI to the resting is very slow due to the reorganization of the  $\mu_3$ -oxo bridge (from  $\text{O}_2$ ) to the external position on the T2 Cu(II). This decay of NI is too slow to be in the catalytic cycle, whereas the reduction of NI is fast ( $>1000\text{s}^{-1}$ )<sup>35</sup> and this is the catalytically relevant fully oxidized form of the MCO's. ET from the T1 to the TNC is fast because the  $\mu_3$ -oxo bridge provides an effective superexchange pathway to the T2 Cu.

#### 4. $\mu_4$ -Sulfide bridged tetranuclear $\text{Cu}_Z$ cluster in Nitrous Oxide Reductase

The tetranuclear  $\text{Cu}_Z$  cluster catalyzes the  $2e^-/2\text{H}^+$  cleavage of the N-O bond in  $\text{N}_2\text{O}$ .<sup>36</sup> From the crystal structure, electrons enter at the mixed valent binuclear  $\text{Cu}_A$  center of one subunit and are transferred over a  $10 \text{ \AA}$  super-exchange pathway to the  $\text{Cu}_Z$  cluster of a 2<sup>nd</sup> subunit where  $\text{N}_2\text{O}$  reduction occurs at the  $\text{Cu}_I/\text{Cu}_{IV}$  edge (Figure 16A). The  $\mu_4\text{SCu}_4$  cluster is held in the protein by 7 His ligands, two on  $\text{Cu}_I$ - $\text{Cu}_{III}$  and one on  $\text{Cu}_{IV}$ . In the resting crystal structures, there are one or two  $\text{H}_2\text{O}$  derived ligands at the  $\text{Cu}_I/\text{Cu}_{IV}$  edge.<sup>36,37</sup>

The initial goal of spectroscopy was to determine the electronic structure of the crystallographically defined resting  $\text{Cu}_Z$  cluster.<sup>38</sup> The  $\text{Cu}_Z$  cluster has a sulfide to Cu CT transition at 640 nm which shows a pseudo-A term MCD spectrum. The temperature dependence of the MCD shows that the ground state has  $S_{\text{tot}}=1/2$ , which can either reflect a site with  $1\text{Cu}^{\text{II}}/3\text{Cu}^{\text{I}}$  or  $3\text{Cu}^{\text{II}}/1\text{Cu}^{\text{I}}$ . These possibilities could be distinguished with XAS at the Cu K-edge, where from Figure 17A the  $\text{Cu}_Z$  feature at 8984 eV shows that 3Cus are reduced in resting  $\text{Cu}_Z$ .<sup>39</sup> This leaves one-hole on the cluster and its distribution could be determined by a combination of X and Q band EPR and S K-edge XAS. Figure 17B shows that the  $g_{\parallel}$  value from Q band lies on a Cu hyperfine line in X band requiring  $e^-$  delocalization over at least 2Cus. These experimental results are supported by geometry optimized DFT calculations (Figure 16B) which show dominant  $\text{Cu}_I$  character but significant delocalization of the hole over the cluster depending on the nature of the edge ligand.<sup>39</sup>

The edge ligand could be detected by rR spectroscopy which also elucidated the requirement of a proton for high activity of  $\text{N}_2\text{OR}$ . A structural model consistent with the results involves an  $\text{OH}^-$  edge ligand whose orientation is affected by H-bonding to a protonated Lys at the  $\text{Cu}_I/\text{Cu}_{IV}$  edge. This protonated Lys appears to play a significant role in assisting catalysis.

We next focus on the redox state of  $\text{Cu}_Z$  required for catalysis. Reduction of the  $\text{Cu}_Z$  EPR signal of the one-hole form directly correlates with the activity. Thus the fully reduced

(4Cu<sup>I</sup>) form of the Cu<sub>Z</sub> reacts with N<sub>2</sub>O in catalysis.<sup>39</sup> Geometry optimization of N<sub>2</sub>O at the Cu<sub>I</sub>/Cu<sub>IV</sub> edge shows that it binds as a μ-1,3 bridge, bent with an angle of 139°. From Figure 18A this bending greatly lowers the energy of the π\* LUMO of N<sub>2</sub>O which leads to extensive backbonding from fully reduced Cu<sub>Z</sub> into the N<sub>2</sub>O activating the cleavage of the N-O bond.<sup>39</sup>

Figure 18B evaluates the potential energy surface for N-O cleavage on the Cu<sub>Z</sub> cluster. The barrier is reduced from 61 kcal/mol in the gas phase to 18 kcal/mol on Cu<sub>Z</sub>. This is because the bent N<sub>2</sub>O reactant is destabilized and, in particular, the extensive backbonding lowers the TS energy through stabilization of the Cu<sub>IV</sub><sup>II</sup>-O<sup>-</sup> bond. Allowing for a protonated ligand to H-bond to this oxo further lowers the TS to ~ 10 kcal/mol. Finally since the two e<sup>-</sup> transferred are donated from Cu<sub>I</sub> and Cu<sub>IV</sub>, it is interesting to evaluate the role of the additional Cus in the cluster. Eliminating Cu<sub>II</sub> and Cu<sub>III</sub> (and saturating the sulfide by protonation) eliminates much of the backbonding into N<sub>2</sub>O and increases the barrier for N-O cleavage to 37 kcal/mol.<sup>40</sup>

The above considerations lead to the molecular mechanism for the 2e<sup>-</sup>/2H<sup>+</sup> cleavage of N<sub>2</sub>O shown in Figure 19. H-bonding from the protonated Lys lowers the barrier for N-O cleavage which leads to the two-hole hydroxyl bridged species. This is rapidly reduced by Cu<sub>A</sub> to the one-hole species where protonation of the Lys again raises the potential and provides a proton to complete the reaction cycle.<sup>40</sup>

## Concluding Comments

Spectroscopic/electronic structural studies on copper proteins, their intermediates and models have provided fundamental insights into their reactivities. Among major issues that remain are the structural differences over the coupled binuclear copper proteins that lead to their different reactivities in Figure 1, whether the side-on structure of oxy-Ty directly reacts with substrates or converts to the bis μ-oxo structure along the reaction coordinate of phenolate binding and hydroxylation in Figure 5, the reactivity of the Cu(II) O<sub>2</sub><sup>-</sup> species in H-atom abstraction and its relevance to the PHM mechanism in Figure 11, the fundamental differences of the trinuclear copper cluster in the multi-copper oxidases relative to the coupled binuclear copper protein sites in dioxygen reactivity and the factors involved in the proton assisted reductive cleavage of the O-O bond, and trapping and defining the key intermediates in the reaction mechanism of N<sub>2</sub>OR in Figure 19. The field of copper bioinorganic chemistry has come a long way, but there is still much to understand.

## Acknowledgements

We thank past students and collaborators who have contributed to this work and the NIH (DK31450) for funding.

## Works Cited

1. Solomon EI, Sundaram UM, Machonkin TE. Multicopper Oxidases and Oxygenases. *Chem Rev* 1996;96:2563–2605. [PubMed: 11848837]
2. Pate JE, Cruse RW, Karlin KD, Solomon EI. Vibrational, electronic, and resonance Raman spectral studies of (Cu<sub>2</sub>(XYL-O)-O<sub>2</sub>)<sup>+</sup>, a copper(II) peroxide model complex of oxyhemocyanin. *J Am Chem Soc* 1987;109:2624–30.
3. Baldwin MJ, Ross PK, Pate JE, Tyeklár Z, Karlin KD, Solomon EI. Spectroscopic and Theoretical Studies of an End-On Peroxide-Bridged Coupled Binuclear Copper(II) Model Complex of Relevance to the Active Sites in Hemocyanin and Tyrosinase. *J Am Chem Soc* 1991;113:8671–8679.
4. Baldwin MJ, Root DE, Pate JE, Fujisawa K, Kitajima N, Solomon EI. Spectroscopic Studies of Side-on Peroxide-Bridged Binuclear Copper(II) Model Complexes of Relevance to Oxyhemocyanin and Oxytyrosinase. *J Am Chem Soc* 1992;114:10421–10431.



5. Metz M, Solomon EI. Dioxygen Binding to Deoxyhemocyanin: Electron Structure and Mechanism of the Spin Forbidden Two-Electron Reduction of O<sub>2</sub>. *J Am Chem Soc* 2001;123:4938. [PubMed: 11457321]
6. Solomon EI, Baldwin MJ, Lowery MD. Electronic Structures of Active Sites in Copper Proteins: Contributions to Reactivity. *Chem Rev* 1992;92:521–542.
7. Solomon EI, Chen P, Metz M, Lee SK, Palmer AE. Oxygen binding, activation, and reduction to water by copper proteins. *Angew Chem Intl Ed* 2001;40:4570–4590.
8. Halfen JA, Mahapatra S, Wilkinson EC, Kaderli S, Young VG, Que L, Zuberbuehler AD, Tolman WB. Reversible Cleavage and Formation of the Dioxygen O-O Bond Within a Dicopper Complex. *Science* 1996;271:1397–1400. [PubMed: 8596910]
9. DuBois JL, Mukherjee P, Collier AM, Mayer JM, Solomon EI, Hedman B, Stack TDP, Hodgson KO. Cu K-edge XAS study of the [Cu<sub>2</sub>(μ-O)<sub>2</sub>] core: Direct experimental evidence for the presence of Cu (III). *J Am Chem Soc* 1997;119:8578–8579.
10. Henson MJ, Mukherjee P, Root DE, Stack TDP, Solomon EI. Spectroscopic and electronic structural studies of the Cu(III)<sub>2</sub> bis-μ-oxo core and its relation to the side-on peroxo-bridged dimer. *J Am Chem Soc* 1999;121:10332–10345.
11. Karlin KD, Nasir MS, Cohen BI, Cruse RW, Kaderli S, Zuberbuehler AD. Reversible Dioxygen Binding and Aromatic Hydroxylation in O<sub>2</sub>-Reactions with Substituted Xylyl Dinuclear Copper(I) Complexes: Syntheses and Low-Temperature Kinetic/Thermodynamic and Spectroscopic Investigations of a Copper Monooxygenase Model System. *J Am Chem Soc* 1994;116:1324–1336.
12. Pidcock E, Obias HV, Zhang CX, Karlin KD, Solomon EI. Investigation of the Reactive Oxygen Intermediate in an Arene Hydroxylation Reaction Performed by Xylyl-Bridged Binuclear Copper Complexes. *J Am Chem Soc* 1998;120:7841–7847.
13. Mirica LM, Vance M, Rudd DJ, Hedman B, Hodgson KO, Solomon EI, Stack TDP. Tyrosinase Reactivity in a Model Complex: An Alternative Hydroxylation Mechanism. *Science* 2005;308:1890–1892. [PubMed: 15976297]
14. Klinman JP. Mechanisms whereby mononuclear copper proteins functionalize organic substrates. *Chem Rev* 1996;96:2541–2561. [PubMed: 11848836]
15. Prigge ST, Kolhekar AS, Eipper BA, Mains RE, Amzel LM. Amidation of bioactive peptides: The structure of peptidylglycine alpha-hydroxylating monooxygenase. *Science* 1997;278:1300–1305. [PubMed: 9360928]
16. Blackburn NJ, Rhames FC, Ralle M, Jaron S. Major changes in copper coordination accompany reduction of peptidylglycine monooxygenase: implications for electron transfer and the catalytic mechanism. *J Bio Inor Chem* 2000;5:341–353.
17. Chen P, Bell J, Eipper BA, Solomon EI. Oxygen activation by the noncoupled binuclear copper site in peptidylglycine alpha-hydroxylating monooxygenase. Spectroscopic definition of the resting sites and the putative Cu<sub>M</sub>(II)-OOH intermediate. *Biochemistry* 2004;43:5735–5747. [PubMed: 15134448]
18. Francisco WA, Wille G, Smith AJ, Merkler DJ, Klinman JP. Investigation of the pathway for inter-copper electron transfer in peptidylglycine alpha-amidating monooxygenase. *J Am Chem Soc* 2004;126:13168–9. [PubMed: 15479039]
19. Chen P, Fujisawa K, Solomon EI. Spectroscopic and theoretical studies of mononuclear copper(II) alkyl- and hydroperoxo complexes: Electronic structure contributions to reactivity. *J Am Chem Soc* 2000;122:10177–10193.
20. Chen P, Root DE, Campochiaro C, Fujisawa K, Solomon EI. Spectroscopic and electronic structure studies of the diamagnetic side-on Cu-II-superoxo complex Cu(O<sub>2</sub>)[HB(3-R-5-iPrpz)<sub>3</sub>]: Antiferromagnetic coupling versus covalent delocalization. *J Am Chem Soc* 2003;125:466–474. [PubMed: 12517160]
21. Chen P, Solomon EI. O<sub>2</sub> activation by binuclear Cu sites: Noncoupled versus exchange coupled reaction mechanisms. *PNAS* 2004;101:13105–13110. [PubMed: 15340147]
22. Prigge ST, Eipper BA, Mains RE, Amzel LM. Dioxygen binds end-on to mononuclear copper in a precatalytic enzyme complex. *Science* 2004;304:864–867. [PubMed: 15131304]

23. Maiti D, Fry HC, Woertink JS, Vance MA, Solomon EI, Karlin KD. A 1:1 Copper-Dioxygen Adduct is an End-on Bound Superoxo Copper(II) Complex which Undergoes Oxygenation Reactions with Phenols. *J Am Chem Soc* 2007;129:264–265. [PubMed: 17212392]
24. Quintanar L, Gebhard M, Wang TP, Kosman DJ, Solomon EI. Ferrous binding to the multicopper oxidases *Saccharomyces cerevisiae* Fet3p and human ceruloplasmin: Contributions to ferroxidase activity. *J Am Chem Soc* 2004;126:6579–6589. [PubMed: 15161286]
25. Messerschmidt A, Ladenstein R, Huber R, Bolognesi M, Avigliano L, Petruzzelli R, Rossi A, Finazziago A. Refined Crystal-Structure of Ascorbate Oxidase at 1.9 Å Resolution. *J Mol Bio* 1992;224:179–205. [PubMed: 1548698]
26. Quintanar L, Yoon J, Aznar CP, Palmer AE, Andersson KK, Britt RD, Solomon EI. Spectroscopic and electronic structure studies of the trinuclear Cu cluster active site of the multicopper oxidase laccase: Nature of its coordination unsaturation. *J Am Chem Soc* 2005;127:13832–13845. [PubMed: 16201804]
27. Shin W, Sundaram UM, Cole JL, Zhang HH, Hedman B, Hodgson KO, Solomon EI. Chemical and spectroscopic definition of the peroxide-level intermediate in the multicopper oxidases: Relevance to the catalytic mechanism of dioxygen reduction to water. *J Am Chem Soc* 1996;118:3202–3215.
28. Sundaram UM, Zhang HH, Hedman B, Hodgson KO, Solomon EI. Spectroscopic investigation of peroxide binding to the trinuclear copper cluster site in laccase: Correlation with the peroxy-level intermediate and relevance to catalysis. *J Am Chem Soc* 1997;119:12525–12540.
29. Bento I, Martins LO, Lopes GG, Carrondo MA, Lindley PF. Dioxygen reduction by multi-copper oxidases; a structural perspective. *Dalt Trans* 2005:3507–3513.
30. Rulisek L, Solomon EI, Ryde U. A combined quantum and molecular mechanical study of the O<sub>2</sub> reductive cleavage in the catalytic cycle of multicopper oxidases. *Inor Chem* 2005;44:5612–5628.
31. Lee SK, George SD, Antholine WE, Hedman B, Hodgson KO, Solomon EI. Nature of the intermediate formed in the reduction of O<sub>2</sub> to H<sub>2</sub>O at the trinuclear copper cluster active site in native laccase. *J Am Chem Soc* 2002;124:6180–6193. [PubMed: 12022853]
32. Aasa R, Branden R, Deinum J, Malmstrom BG, Reinhammar B, Vanngard T. A <sup>17</sup>O-effect on EPR spectrum of intermediate in dioxygen-Laccase reaction. *BBRC* 1976;70:1204–1209. [PubMed: 182162]
33. Yoon J, Mirica LM, Stack TDP, Solomon EI. Spectroscopic demonstration of a large antisymmetric exchange contribution to the spin-frustrated ground state of a D<sub>3</sub> symmetric hydroxy-bridged trinuclear Cu(II) complex: Ground-to-excited state superexchange pathways. *J Am Chem Soc* 2004;126:12586–12595. [PubMed: 15453791]
34. Yoon J, Mirica LM, Stack TDP, Solomon EI. Variable-temperature, variable-field magnetic circular dichroism studies of tris-hydroxy- and μ<sub>3</sub>-oxo-bridged trinuclear Cu(II) complexes: Evaluation of proposed structures of the native intermediate of the multicopper oxidases. *J Am Chem Soc* 2005;127:13680–13693. [PubMed: 16190734]
35. Cole JL, Ballou DP, Solomon EI. Spectroscopic characterization of the peroxide intermediate in the reduction of dioxygen catalyzed by the multicopper oxidases. *J Am Chem Soc* 1991;113:8544–8546.
36. Zumft WG, Kroneck PMH. Respiratory transformation of nitrous oxide (N<sub>2</sub>O) to dinitrogen by bacteria and archaea. *Advances in microbial physiology* 2006;52:107–227. [PubMed: 17027372]
37. Brown K, Tegoni M, Prudencio M, Pereira AS, Besson S, Moura JJ, Moura I, Cambillau C. A novel type of catalytic copper cluster in nitrous oxide reductase. *Nat Struct Biol* 2000;7:191–195. [PubMed: 10700275]
38. Rasmussen T, Berks BC, Sanders-Loehr J, Dooley DM, Zumft WG, Thomson AJ. The catalytic center in nitrous oxide reductase, Cu<sub>z</sub>, is a copper-sulfide cluster. *Biochemistry* 2000;39:12753–12756. [PubMed: 11041839]
39. Chen P, Gorelsky SI, Ghosh S, Solomon EI. N<sub>2</sub>O reduction by the μ<sub>4</sub>-sulfide-bridged tetranuclear Cu<sub>z</sub> cluster active site. *Angew Chem Intl Ed* 2004;43:4132–40.
40. Gorelsky SI, Ghosh S, Solomon EI. Mechanism of N<sub>2</sub>O Reduction by the μ<sub>4</sub>-S Tetranuclear Cu<sub>z</sub> Cluster of Nitrous Oxide Reductase. *J Am Chem Soc* 2006;128:278–290. [PubMed: 16390158]

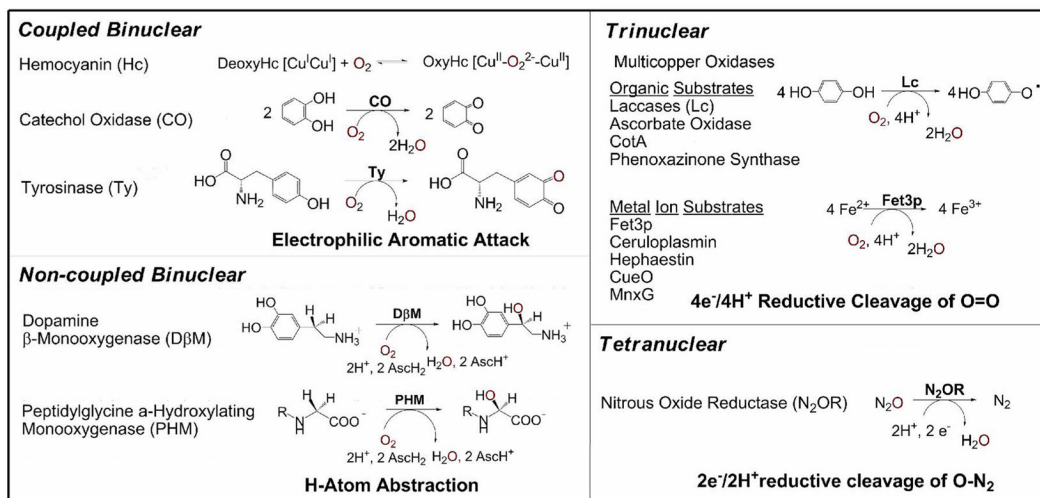


**Figure 1.**  
Multinuclear Cu Sites in Biology

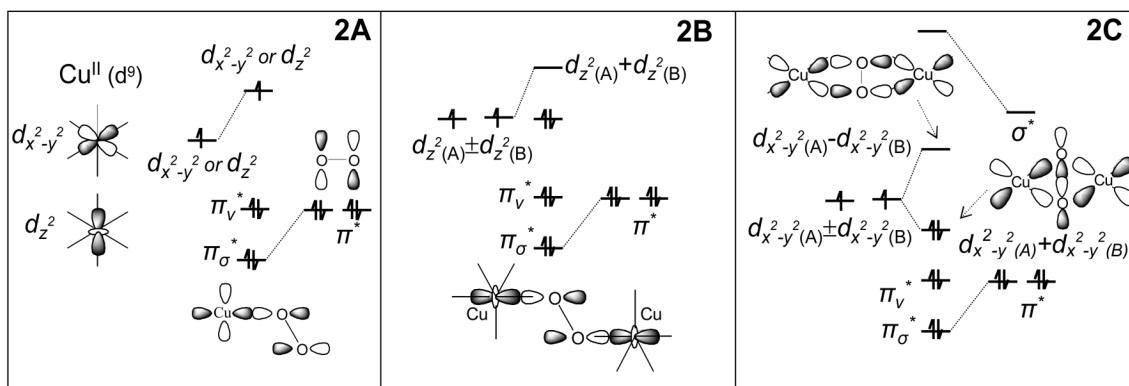


**Figure 2.** Electronic structure of (A) End-on  $\text{Cu-O}_2^{2-}$  complex (B) End-on bridged  $[\text{Cu}_2\text{-O}_2^{2-}]$  complex and (C) Side-on bridged OxyHc.

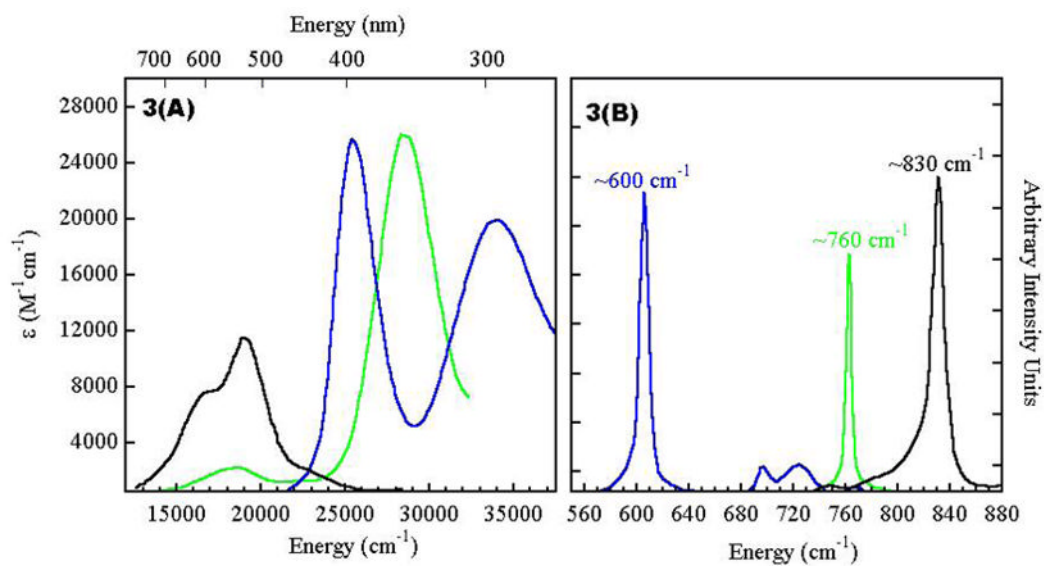


**Figure 3.** (A) Absorption and (B) Resonance Raman spectra of  $\{[(TMPA)Cu]_2O_2\}^{2+}$  (end-on) (—),  $Cu[HB(3,5-i-Pr_2pz)_3]_2(O_2)$  (side-on) (—) and  $\{[L^{TMCHD}Cu]_2O_2\}$  (bis- $\mu$ -oxo) (—)

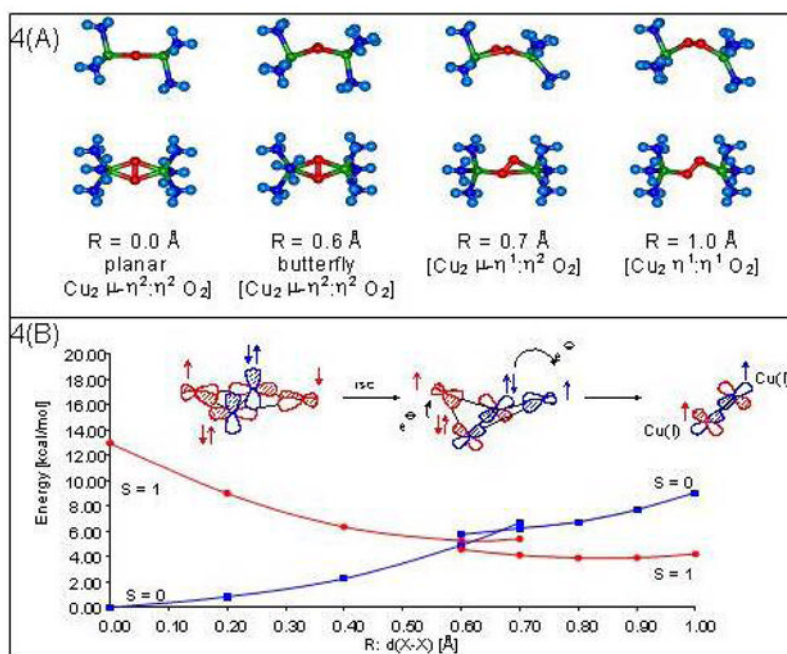


**Figure 4.** (A) The reaction coordinate of O<sub>2</sub> binding by Hc. View along the O-O (Top) and perpendicular to initial Cu<sub>2</sub>O<sub>2</sub> plane (bottom). (B) Potential-energy surfaces for the interconversion of OxyHc and DeoxyHc in triplet and Singlet state. R:d(X-X) is the distance between the center of the O-O and Cu-Cu vectors. R:d(X-X) <~0.6 and >~0.6 represents symmetric and non-symmetric O<sub>2</sub> coordination, respectively.

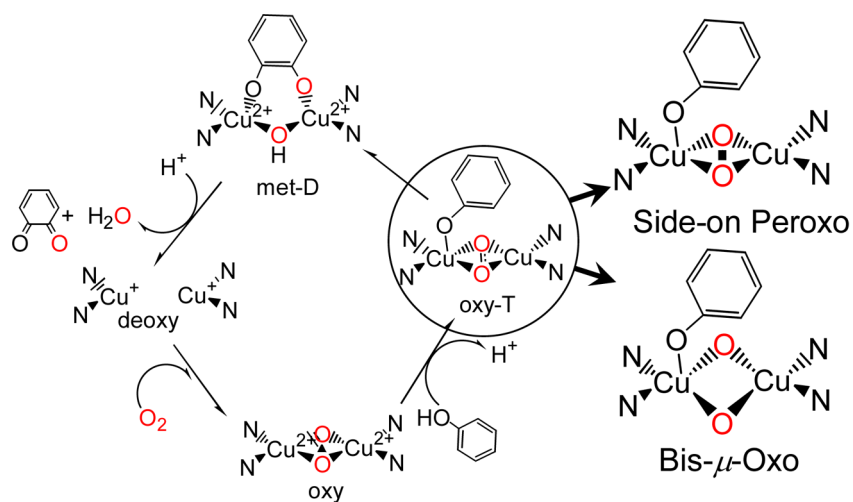


**Figure 5.** Molecular mechanism of Ty catalysis. The two possible structures of substrate bound oxy-T are expanded.

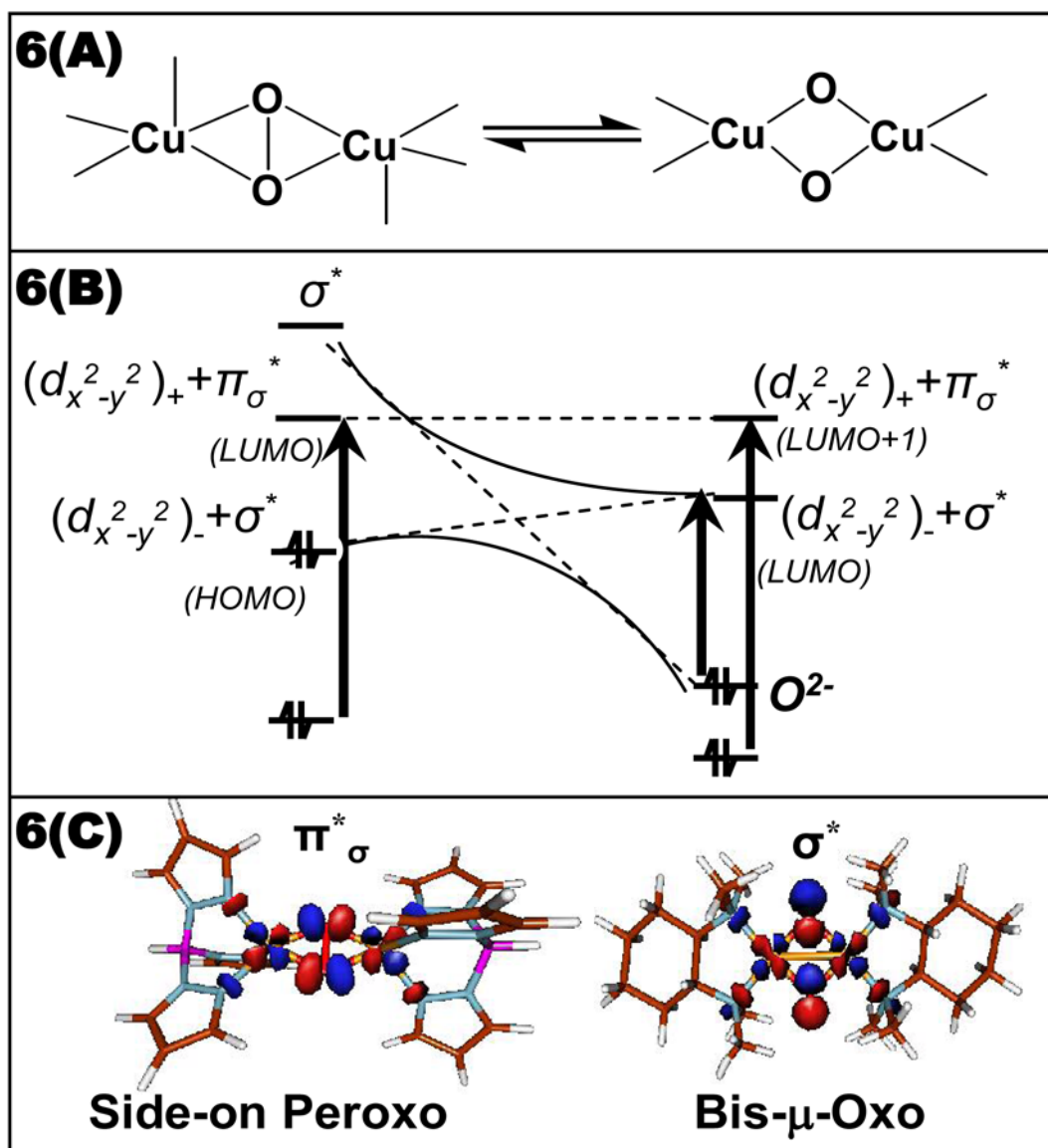


**Figure 6.** (A) Side-on peroxo (left), Bis- $\mu$ -Oxo (right) correlation (B) electronic structure correlation (C) FMO's (ie. LUMO's).



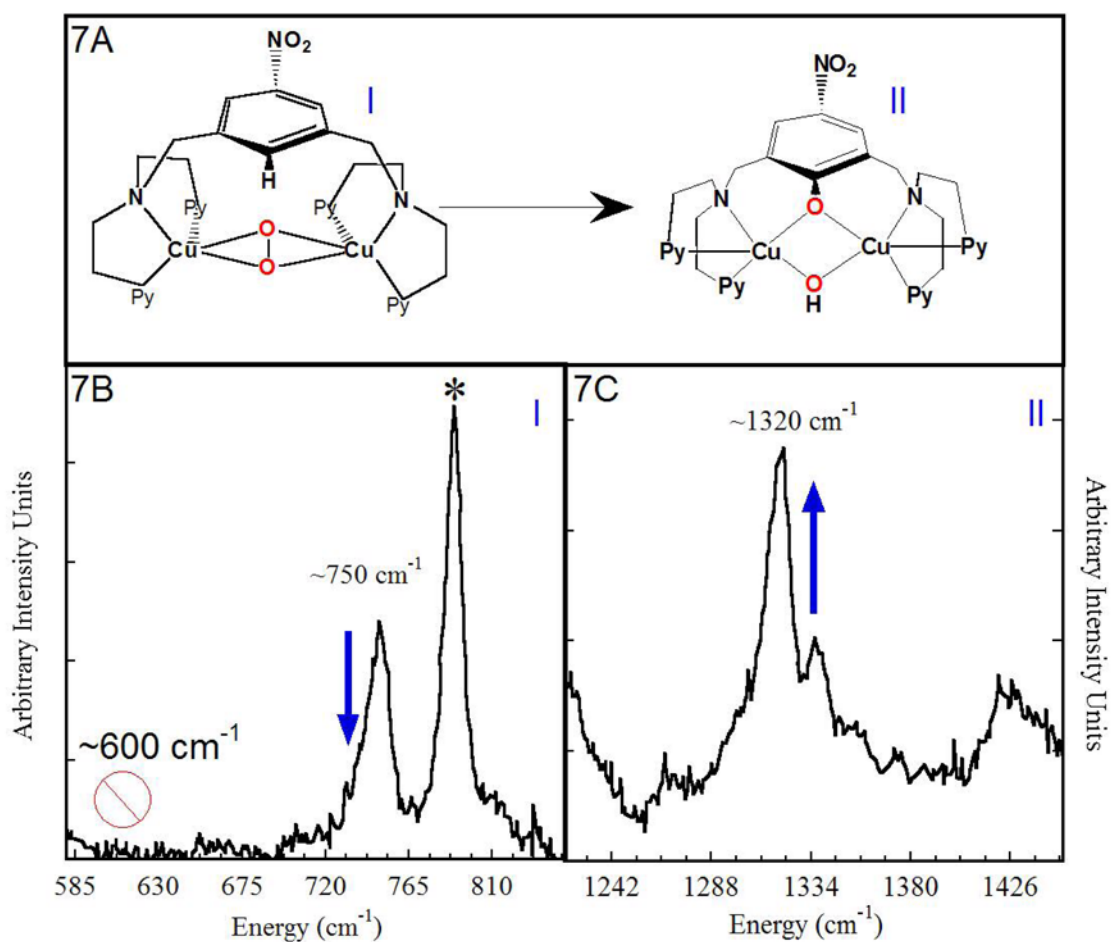


**Figure 7.**

(A) Conversion of the side-on peroxide intermediate  $[\text{Cu}_2(\text{NO}_2\text{-XYL})(\text{O}_2)]^{2+}$  to  $[\text{Cu}^{\text{II}}_2(\text{NO}_2\text{-XYL-O}^-)(\text{OH})]^{2+}$ . (B) & (C) Change in rR with time: loss of side-on peroxo stretch correlates with increase of C-O stretch.

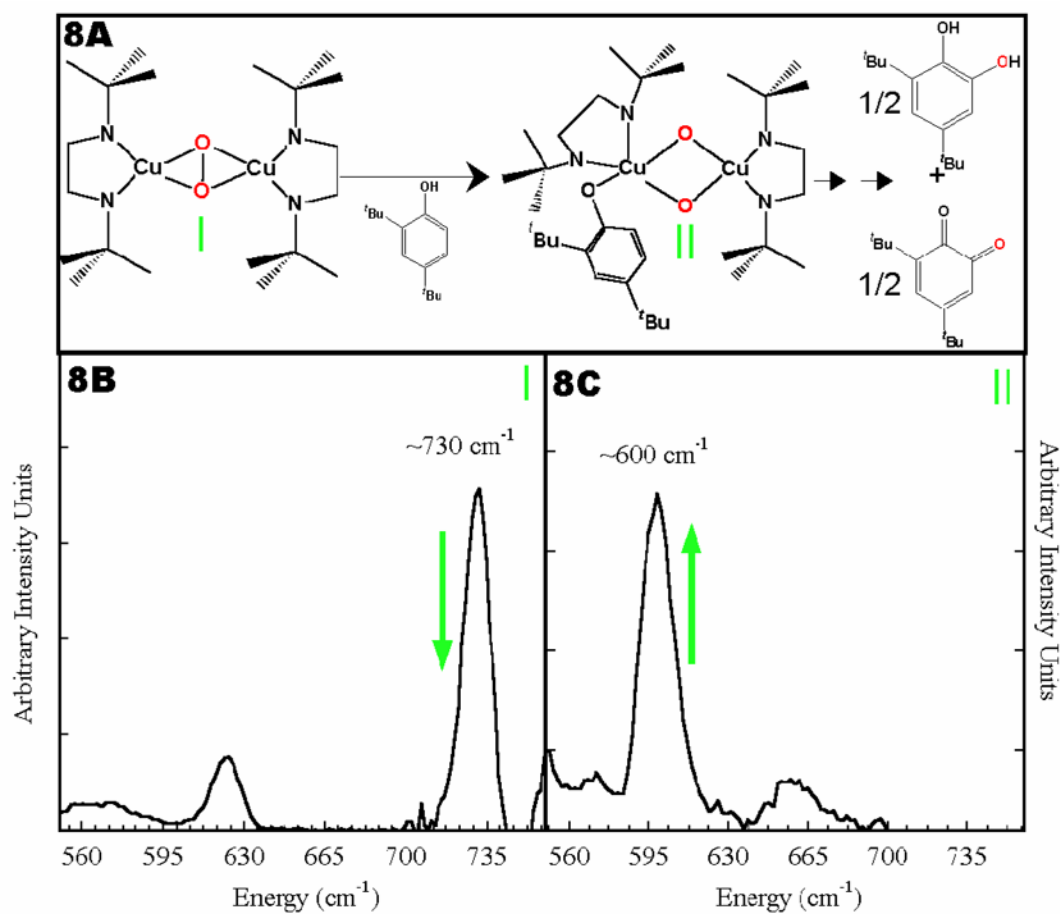


**Figure 8.** (A) Reaction of Side-on peroxo  $\{[(DBED)Cu]_2O_2\}^{2+}$ . (B) & (C) Change in rR with  $(tBu)_2Ph(O^-)$  coordination.

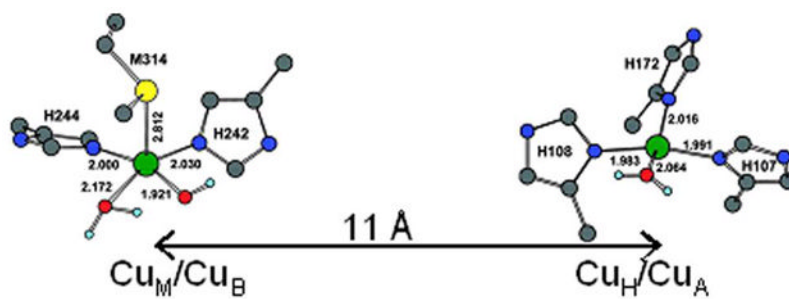


**Figure 9.** Geometry-optimized structures of the resting oxidized  $\text{Cu}_M$  and  $\text{Cu}_H$  sites in PHM.

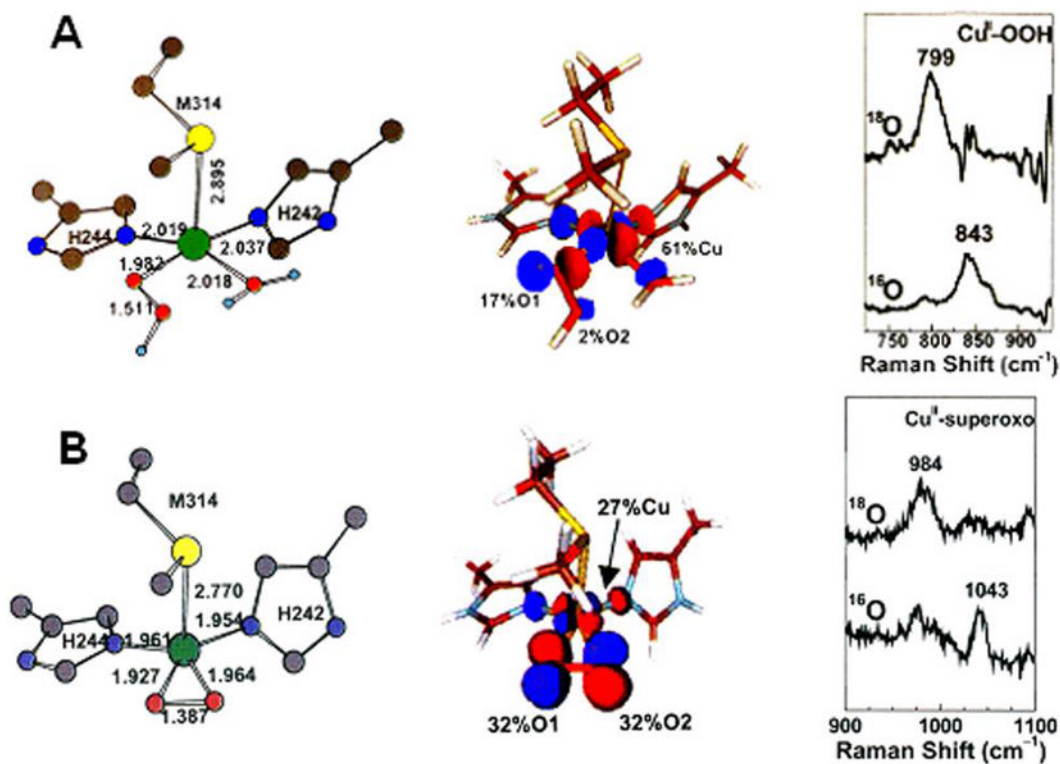


**Figure 10.** Electronic structure of the Cu<sup>II</sup><sub>M</sub>-OOH (A) and Cu<sup>II</sup><sub>M</sub>-superoxo (B) species. Geometry-optimized structure (left), acceptor FMO (LUMO) (middle), rR spectra in  $\nu_{O-O}$  region (right).

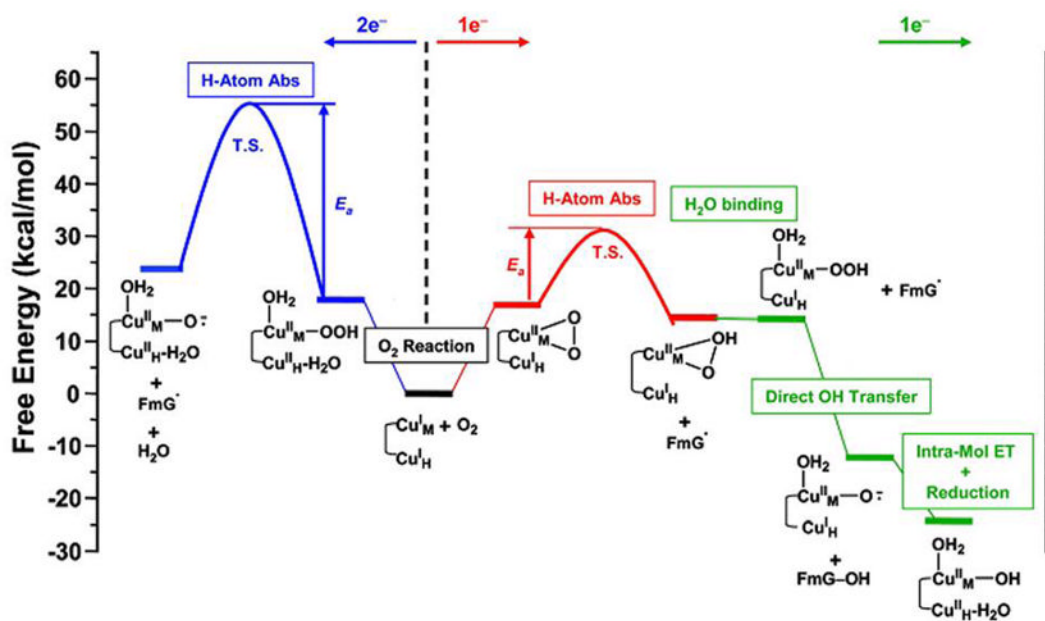


**Figure 11.**  
 Summary of the  $2e^-$  (blue) and  $1e^-$  (red, green) reaction coordinates for the non-coupled binuclear Cu enzymes.

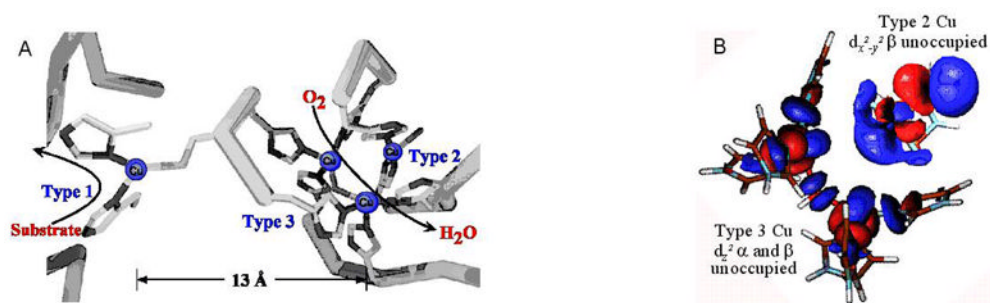


**Figure 12.**  
(A) Active site of the MCO's (AO is shown here) (B) electronic structure of the TNC.

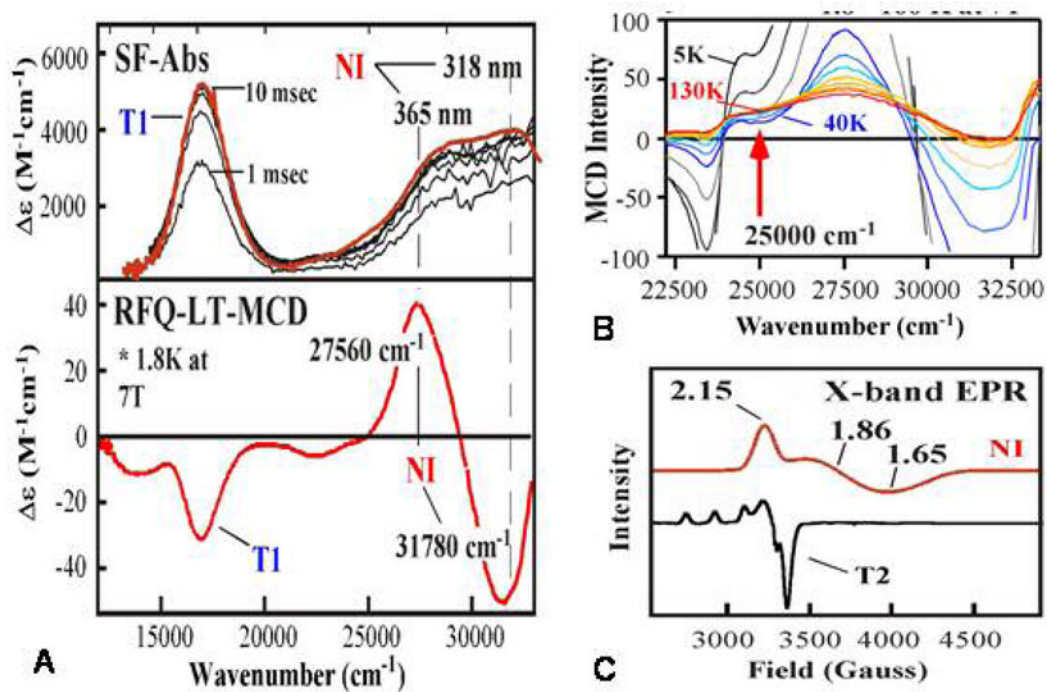


**Figure 13.**

(A) Stopped-flow absorption showing the formation of NI, (B) RFQ-LT-MCD spectrum of NI, (C) VTMCD of NI, and (D) low temperature X-band EPR spectrum of NI compared to resting T2.

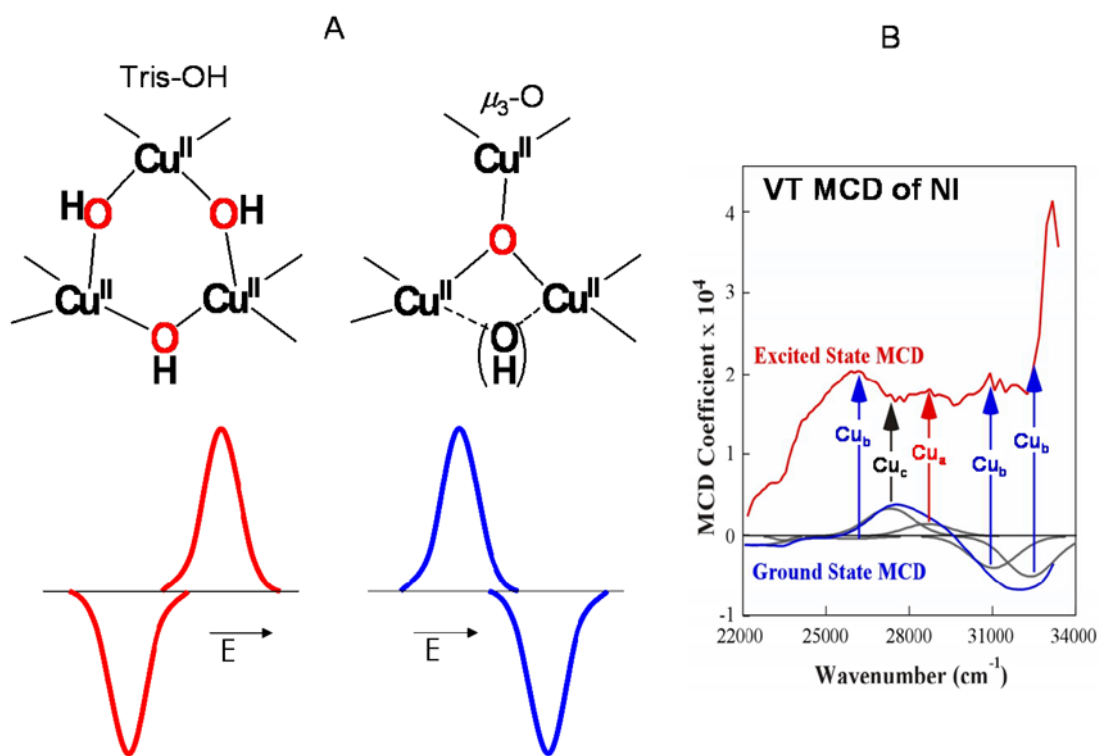


**Figure 14.** (A) Predicted and observed MCD signs for the two possible structures of NI and (B) ground and excited state MCD spectra of NI, where bands are grouped together according to their different temperature dependencies



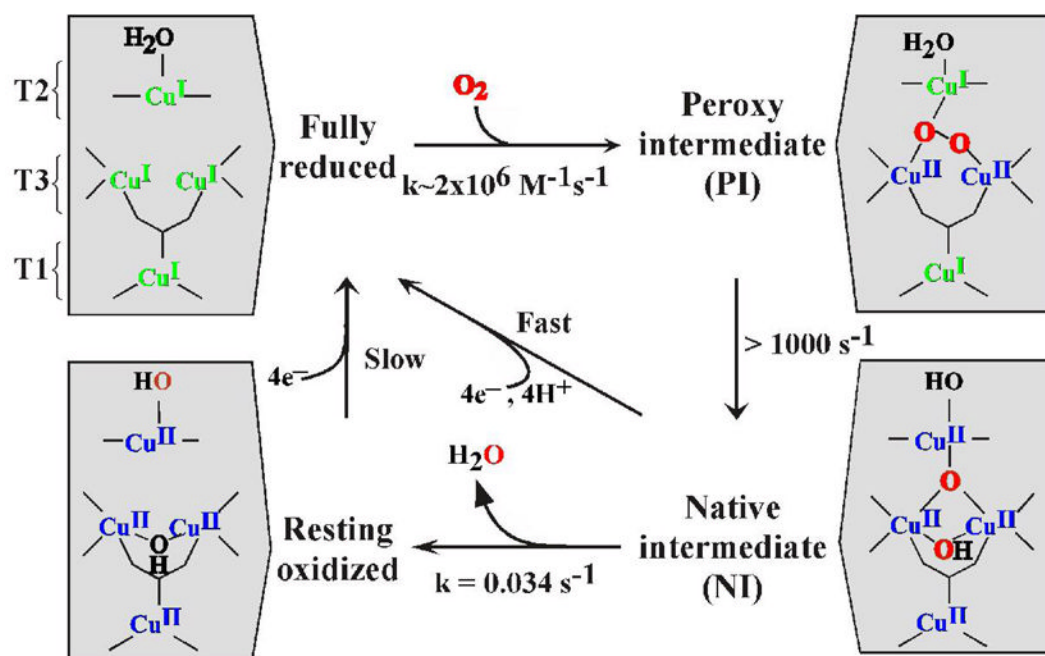
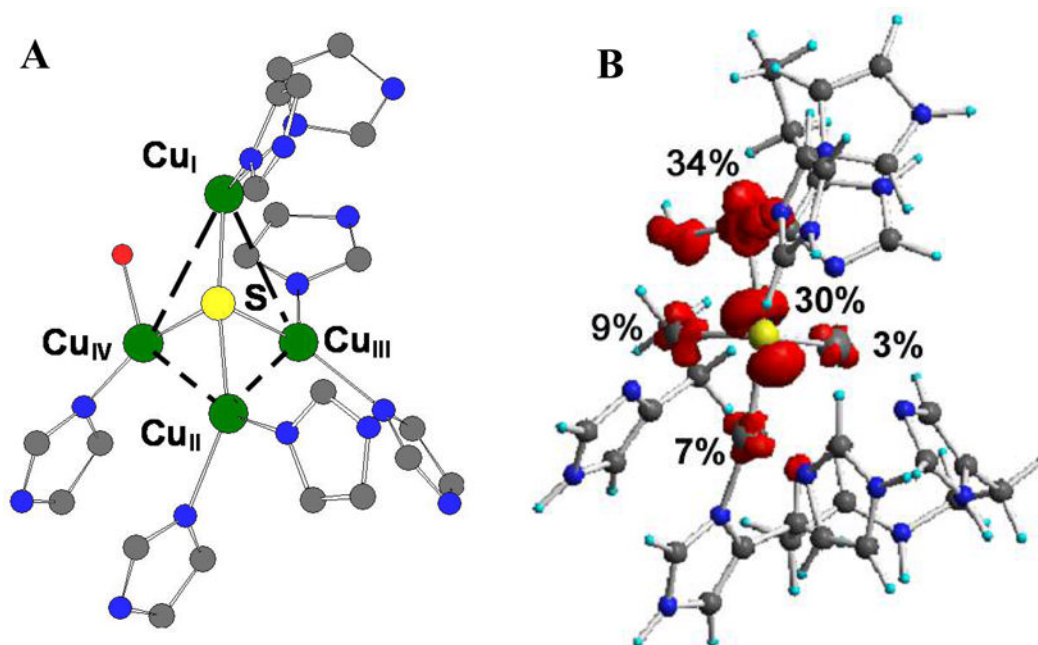


Figure 15.  
MCO mechanism



**Figure 16.**  
(A) Crystal structure (PnN<sub>2</sub>OR) (B) Geometry optimized electronic structure

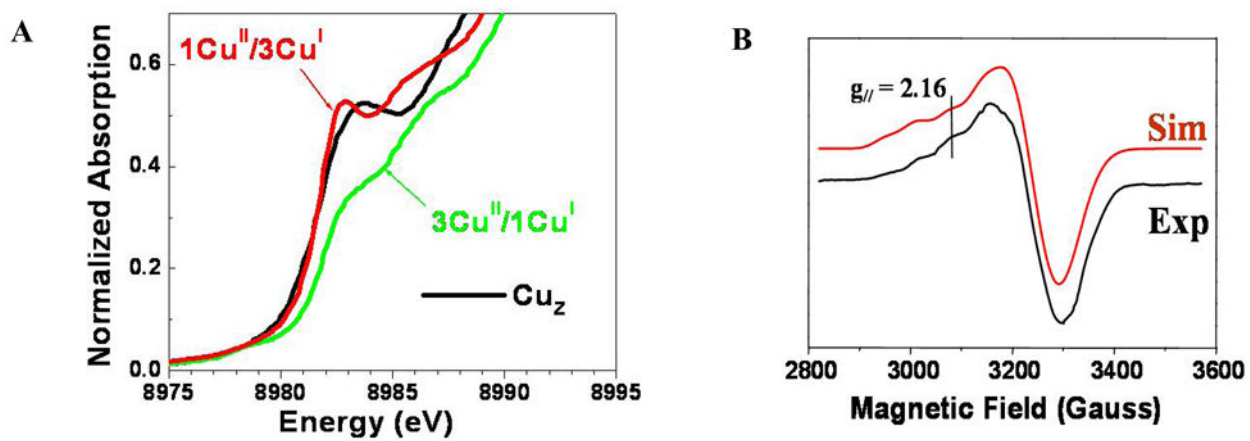
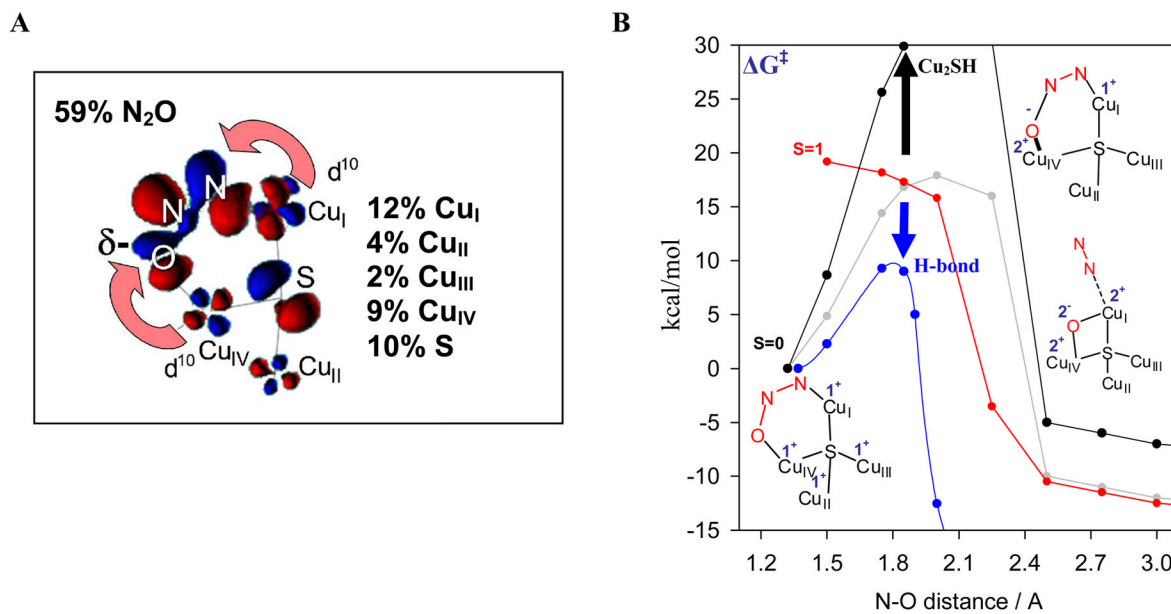
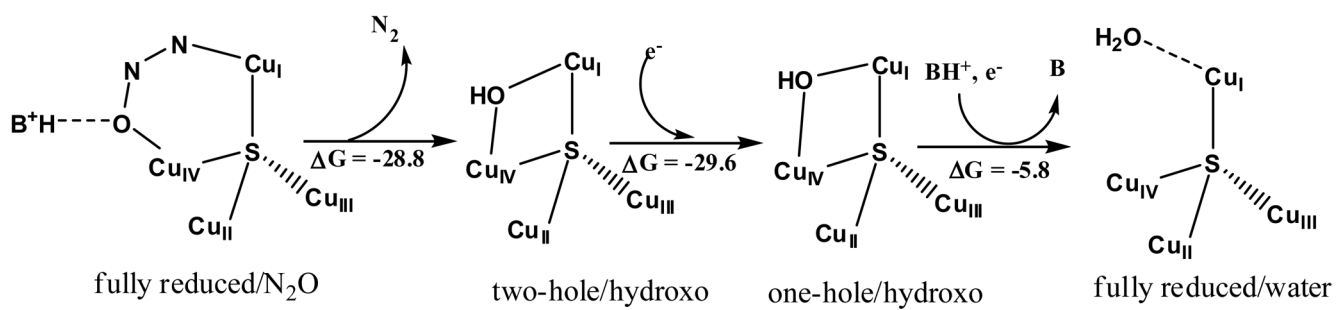


Figure 17.  
(A) Cu-K edge XAS spectrum of  $\text{Cu}_2$  (black) simulated with  $1\text{Cu}^{\text{II}}/3\text{Cu}^{\text{I}}$  and  $3\text{Cu}^{\text{II}}/1\text{Cu}^{\text{I}}$  (B) EPR spectrum of  $\text{Cu}_2$  from  $\text{PnN}_2\text{OR}$



**Figure 18.** (A) Backbonding interaction from fully reduced  $\text{Cu}_2$  to  $\text{N}_2\text{O}$  (B) N-O bond cleavage barrier of  $\text{Cu}_2$  (red/grey),  $\text{Cu}_2\text{SH}$  (black), H-bond assisted (blue).



**Figure 19.**  
 $N_2OR$  reaction mechanism